JTTEE5 7:537-545

PEER REVIEWED

Oxidation in Wire HVOF-Sprayed Steel

R.A. Neiser, M.F. Smith, and R.C. Dykhuizen

(Submitted 16 January 1998; in revised form 13 May 1998)

It is widely held that most oxidation in thermally sprayed coatings occurs on the surface of the droplet after it has flattened. Evidence in this paper suggests that, for the conditions studied here, oxidation of the top surface of flattened droplets is not the dominant oxidation mechanism. In this study, a mild steel wire (AISI 1025) was sprayed using a high-velocity oxy-fuel (HVOF) torch onto copper and aluminum substrates. Ion milling and Auger spectroscopy were used to examine the distribution of oxides within individual splats. Conventional metallographic analysis was also used to study oxide distributions within coatings that were sprayed under the same conditions. An analytical model for oxidation of the exposed surface of a splat is presented. Based on literature data, the model assumes that diffusion of iron through a solid FeO layer is the rate limiting factor in forming the oxide on the top surface of a splat. An FeO layer only a few nanometers thick is predicted to form on the splat surface as it cools. However, experimental evidence shows that the oxide layers are typically 100× thicker than the predicted value. These thick oxide layers are not always observed on the top surface of a splat. Indeed, in some instances the oxide layer is on the bottom, and the metal is on the top. The observed oxide distributions are more consistently explained if most of the oxide forms before the droplets impact the substrate.

Keywords Auger spectroscopy, HVOF, oxidation

1. Introduction

Oxidation of thermally sprayed metals can significantly influence the phase composition, microstructure, properties, and performance of sprayed coatings. In many applications metal oxides (often concentrated along splat boundaries) tend to degrade the properties and performance of metal coatings. Degradation can be caused by many factors: for example, molten metals typically do not wet or adhere well to metal oxides causing poor intersplat cohesion; the metal oxides tend to be brittle, have different thermal expansion coefficients than the surrounding metal, and disrupt the chemical uniformity of surfaces exposed to corrosive environments. However, in some cases metal oxides in the sprayed coatings have also been found to enhance certain properties. For example, in the case of mild steel wire high-velocity oxy fuel (HVOF) sprayed onto the cylinder walls of aluminum automobile engines, it was found that metal oxides formed in the deposition process contribute to the wear resistance of the coating (Ref 1).

Regardless of whether oxidation is viewed as "good" or "bad" for a specific application, it is clearly desirable to be able to control the extent of oxide formation. While this can be accomplished reasonably well with chambered spray processes, such solutions are cost prohibitive for many applications. Mechanical shrouds or inert gas shrouded spray systems are less expensive but provide a lesser degree of control over the oxidation processes. If we can better understand how and where oxidation occurs during thermal spray deposition, then we should be able to develop better, more cost-effective ways to control it.

R.A. Neiser, M.F. Smith, and **R.C. Dykhuizen,** Sandia National Laboratories, Albuquerque, NM 87185-1130. Contact M.F. Smith at e-mail: mfsmith@sandia.gov.

1.1 Some Previous Studies on Oxide Formation

Previous studies have explored many aspects of oxide formation for various materials and spray processes. In such studies, it is common to consider three regions where oxidation can occur: 1) the "core" region of the oxy-fuel flame or plasma jet (typically similar in extent to the highly luminous portion of the flame or jet) where oxygen from the ambient atmosphere has not penetrated yet, 2) the "free jet" portion of the spray plume (extending from the core region to the substrate surface) where process gases and the ambient atmosphere become intermixed, and 3) the "surface" region (surface of a recently deposited splat prior to significant cooling) where hot metal is exposed to a mixture of effluent from the spray process and the ambient atmosphere.

Swank et al. (Ref 2) studied oxidation in an HVOF system using Inconel powder. They concluded that little oxidation occurred in-flight and that most of the oxidation occurred on the substrate. This conclusion was based on the fact that the oxide levels were only a function of the substrate temperature, and not the amount of entrained air or excess combustion oxygen. However, their particle temperature data reveal that the average particle was not molten in-flight. Thus, the splats, with a higher surface-to-volume ratio, would naturally oxidize faster than the in-flight particles. Creffield et al. (Ref 3) experimentally showed that the oxide level in a WC-Co coating deposited with a powder fed HVOF process did vary with the oxygen content of the combustion gases. However, they did not determine where the oxidation occurred.

In a study by Hackett and Settles (Ref 4), pure iron powder (highly susceptible to oxide formation) was HVOF spray deposited in ambient atmospheres of pure nitrogen, 92% nitrogen/8% oxygen, and 80% nitrogen/20% oxygen (similar to ambient air). For the conditions of their study, they found that spraying in an inert gas environment reduced the exothermic oxidation heating of the spray particles, as evidenced by reduced luminescence of the particles in the spray plume. They were also able to reduce

the oxide levels in HVOF coatings by as much as 50% by spraying with a ducted shroud of inert gas. Their results showed that the amount of oxide in the coating increased linearly with ambient oxygen concentration, and they concluded that approximately 75% of the oxide formation occurred after the particles left the core region (i.e., in the free jet and/or on the splat surface). These results were consistent with their results from an earlier study (Ref 5) in which the gas flux of the HVOF jet 30 to 40 cm downstream of the nozzle exit was found to be at least a factor of 10 above the initial gas flux at the nozzle exit. Hence, these investigators concluded that the gas surrounding the particles during flight and after splat impact is only about 10% combustion products and 90% ambient atmosphere.

1.2 The Role of High Oxygen Concentrations

The concept of high oxygen concentrations in an HVOF spray plume and at the coating surface is further supported by solid electrolyte oxygen probe measurements by Korpiola et al. (Ref 6). These authors found that oxygen concentrations in an HVOF spray plume increased with increasing distance from the nozzle exit. Their measurements indicated "unexpectedly high" oxygen concentrations of 4 to 17 mol%, (depending upon the hydrogen fuel to oxygen ratio) at a distance of 150 mm downstream from the nozzle exit. These investigators concluded that the oxygen concentration in the HVOF spray plume is so high, even with a reducing flame of four parts hydrogen to one part oxygen, the excess hydrogen does not provide protection against coating oxidation at normal standoff distances.

Since the oxygen content of the flame increases with distance, one might expect greater coating oxidation at longer standoff distances. However, Hackett and Settles (Ref 5) found that oxide content in the coating decreased with increasing torch-to-workpiece distance. This was explained by the fact that oxidation was also found to decrease sharply with decreasing substrate temperature, and the substrates at longer standoff distances were cooler. The dominance of surface temperature as the key factor affecting oxidation led Hackett and Settles to conclude that splat surface oxidation after impact was the dominant oxidation mechanism for the conditions of their experiments.

In a similar study of oxidation for the case of plasma sprayed iron powder, Vardelle, Fauchais, and Themelis (Ref 7) considered equations that should describe the rate-controlling phenomena for oxidation mechanisms in the free jet and on the splat surface. These investigators also concluded that oxidation probably occurs primarily during the time of exposure of the hot splat surface to the process gas jet and to the ambient atmosphere, before this splat surface is covered by other impinging splats and before the splat surface has cooled significantly.

1.3 HVOF Spray Devices

These previous studies with powder-fed spray devices suggest that oxidation occurs primarily after impact and on the surface of a hot splat. This does not seem unreasonable, because cold, initially unmelted particles are being injected, and the total time available for in-flight oxidation would typically be on the order of only a few milliseconds. Additionally and perhaps more importantly, the splats have a much larger surface-to-volume ratio than the droplets. However, Hackett and Settles observations that particle luminescence decreased when an inert gas shroud was used indicates that sufficient exothermic in-flight oxidation did occur to raise the temperature and luminescence of the spray particles. This is supported by observations during the present study that particle luminescence and measured in-flight droplet temperatures increase when a HVOF torch is operated under oxygen-rich conditions, suggesting that exothermic in-flight oxidation causes significant droplet heating.

Unlike the powder-fed HVOF devices in the studies just described, a wire-fed HVOF torch (Fig. 1) was used in the present study. In a powder-fed system, cold solid powder particles are injected and melting occurs in-flight. But in a wire-fed system, high-speed video imaging shows that the droplets are already fully molten when they leave the wire tip (Ref 8). Since the most likely surface oxide (FeO) has a melting point (1644 K) that is lower than the melting point of pure iron (1805 K), we would expect any surface oxide to also be fully molten. Under these conditions, some approximate fluid dynamic calculations (see Appendix) suggest that shear forces caused by the gas flow across the molten surface of the droplet may cause significant fluid flow and mixing within the droplet while it is in flight. (It is noteworthy that some other metals form oxides that melt at much higher temperatures relative to the pure metal. Hence, for some other spray conditions, the surface oxide on the droplets might be solid rather than liquid.)

In a wire-fed HVOF device, oxidation can occur: 1) on the wire, before the molten metal is stripped off, 2) in-flight, 3) on the splat surface, and 4) in "splashed" material that is incorporated into the coating (i.e., molten material that is ejected from the main droplet upon impact, forming smaller "sub-droplets" with a higher surface-to-volume ratio). Because the steel droplets in the wire-fed device start out hot and fully molten, with possible in-flight fluid flow and mixing to constantly expose fresh molten metal at the droplet surface, it seems reasonable to expect that there might be increased in-flight oxidation in the present study as compared to the prior work with powder-fed spray devices. However, it is difficult to separate and quantify the relative contributions of different oxidation mechanisms. In this study, we investigated the oxide distribution within individual splats to learn more about oxidation mechanisms.

1.4 The Distribution of Oxides within a Coating

The distribution of oxide within individual splats might indicate whether oxidation occurred primarily before or after droplet impact. If oxidation occurs primarily on the hot splat surface after impact, then one might expect most of the oxide to be localized along the exposed surface of the splat (i.e., the side away

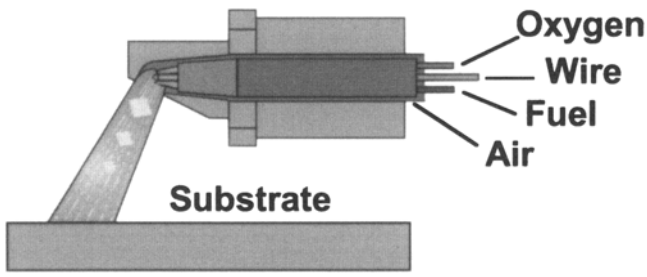

Fig. 1 Schematic of the wire-fed HVOF spray torch

from the substrate). One would also expect comparatively little oxygen to be present in the interior of the splat or along the bottom surface of the splat adjacent to the substrate. If, on the other hand, the molten iron oxidized primarily on the wire or in-flight, possibly with some shear-induced fluid flow and mixing, then a different distribution might be expected. Pre-impact oxidation might produce a more uniform distribution of oxide throughout the splat, perhaps with some localized segregation of molten iron or iron oxide (much like droplets of oil segregated in water) that could cause highly localized "pockets" of pure iron or pure oxide in the final splat. Such phase segregation in the liquid droplet is likely because the iron-oxygen phase diagram indicates that liquid mixtures of Fe and FeO remain immiscible at temperatures well beyond 2000 K, the highest temperature reported on the phase diagram (Ref 9).

In the present study, oxygen concentration profiles were experimentally measured as a function of depth through the entire thickness of individual splats. The observations then were compared to a simple analytical model of the expected surface oxide thickness with the assumption that oxidation occurred primarily on the splat surface after impact and solidification. The oxygen concentration profiles were measured by alternately using ion sputtering to remove material in very thin, incremental layers from an individual splat and, after each sputtering cycle, measuring the oxygen concentration at the surface of the ion milled region with Auger Electron Spectroscopy (AES).

2. Experimental Procedure

2.1 Sample Preparation

The wire-fed HVOF device used in this study is similar to a Metco Diamond Jet Rotary Wire (DJRW; Sulzer Metco of Westbury, New York) system. As shown in Fig. 1, the steel wire is fed down the central axis of the torch, and an oxy-fuel flame continuously melts the tip of the wire. A sheath of compressed air is injected around the interior perimeter of the combustion chamber to form a cold air boundary layer that cools the spray torch. This injected air flow also raises the total combustion chamber pressure in order to achieve supersonic gas flows in the rapidly expanding gas jet as it exits the spray device. The outer portion of the spray torch rotates about the central axis of the torch, thus producing a rotating spray of molten metal that can be used to coat the internal diameter of a pipe or cylinder. A computational fluid dynamics analysis of this torch has been presented previously (Ref 10).

For this study, 3.2 mm diam AISI 1025 steel wire was sprayed onto 50 mm long by 13 mm wide by 3.2 mm thick copper and aluminum plates. The plates were lightly sanded to roughen the surface for better adhesion and then cleaned with acetone and methanol. The plates were oriented such that the spray distance from the tip of the wire along the droplet flight path to the substrate surface was approximately 5 cm. In order to explore droplet oxidation under oxygen-rich conditions, the coatings were sprayed using an oxygen/fuel stoichiometric ratio of $\Phi = 2$ (i.e., twice the stoichiometric amount of oxygen). The total oxy/fuel flow was 236 liters/min (500 SCFH) and the flow of compressed air was 660 liters/min (1400 SCFH). The torch was rotated at 800 rev/min, and the rotating torch was rapidly traversed (25 cm/s) once across the central region of the plate in a direction normal to the page in Fig. 1. This procedure produced a thin stripe of coating across the metal plates. After finishing the spray run, each sample was put into a plastic bag filled with argon.

Individual splats were used for the AES analyses, because we could then use the change in composition from iron to the substrate metal to determine when we had ion milled completely through an individual splat. Individual splats could not be picked out from the central region of the sprayed stripe, but individual splats were plentiful on the periphery of the stripe.

Coatings were also produced at the same spray conditions for metallographic and oxygen analysis. The coatings were sprayed onto aluminum substrates and the rotating torch was traversed from left to right in Fig. 1. A phase Doppler particle analyzer (PDPA) was used to measure in-flight droplet size and velocity distributions in the spray plume at the 5 cm standoff distance in a manner similar to that described previously (Ref 11). The volumetric sizes had an essentially log-normal distribution, with a volumetric average droplet size of 48 μm and a geometric standard deviation of 1.4 (note: A geometric standard deviation is a dimensionless number that describes the width of a log-nominal distribution. See Ref 11).

2.2 Sample Analysis

The samples were handled with lint free gloves so they could be directly placed in the vacuum chamber of an Auger spectroscopy/ion milling instrument (Fig. 2). All data were obtained with a Physical Electronics PHI660 scanning auger operating at an acceleration voltage of 5 keV and a beam current of 1 μA, producing an estimated spot size of ~1 μm. Ion sputtering for the depth profiles was performed using a rastered 3 keV Xenon ion beam that produced a sputter rate of 21.7 nm/min for an SiO_2 reference standard.

Elemental concentration profiles were measured by alternately sputtering a selected region of an individual splat and then measuring the concentrations at the base of the sputter "crater" with Auger analysis. An advantage of AES for this type

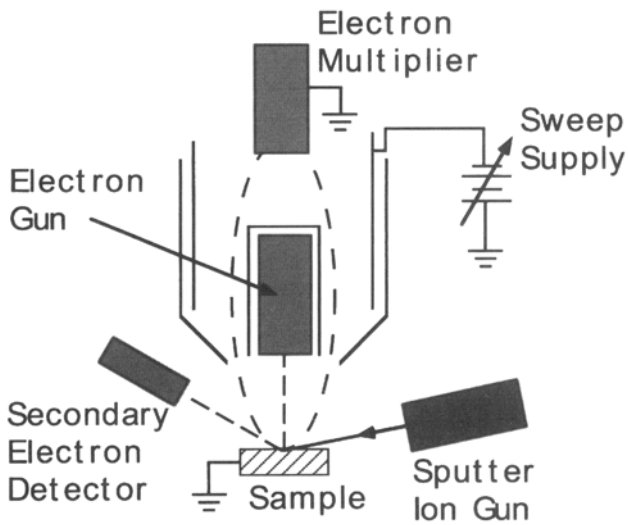

Fig. 2 Schematic of the Auger ion milling apparatus

of profiling is that the depth of the sample volume that is analyzed is shallow, typically ~1 nm. Because the splat thickness and the true sputtering rate through the splat material were both unknown, the appearance of the substrate metal in the Auger spectra was used as an indication that the bottom of the splat had been reached by ion milling. A small increase in the oxygen

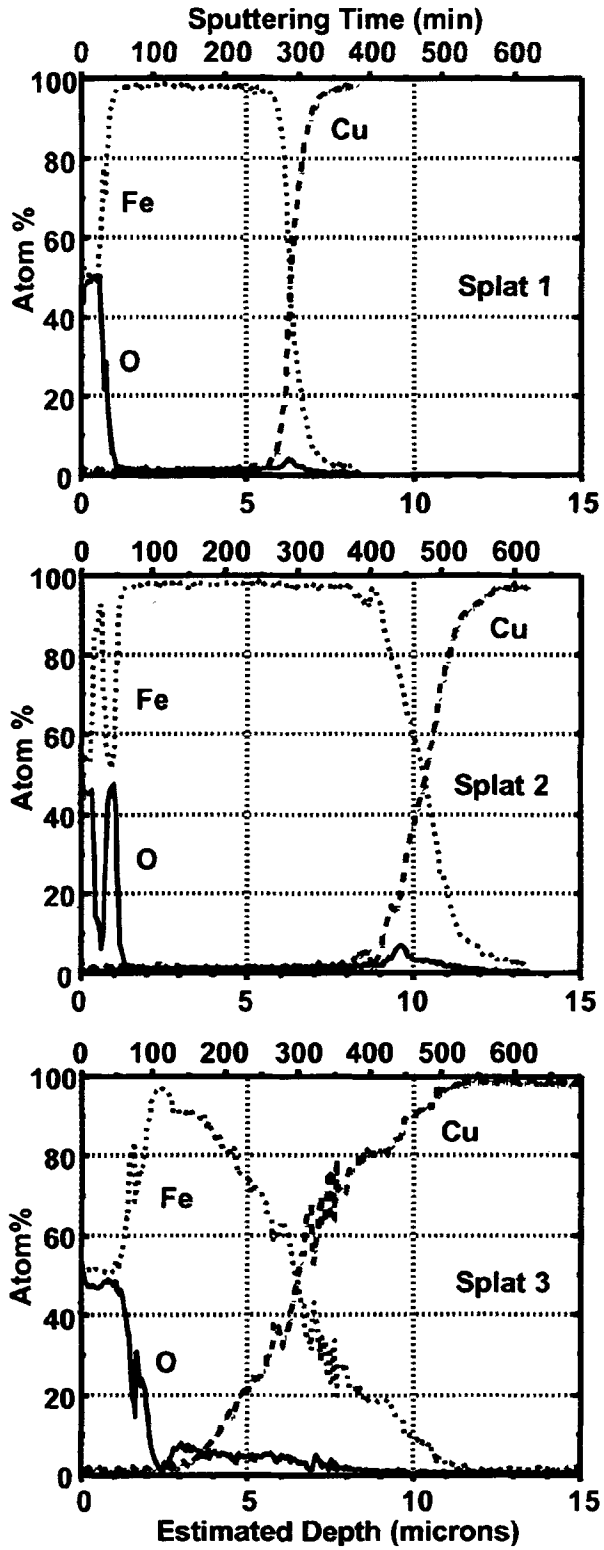

Fig. 3 Concentration profiles through three splats. The sputtering time axis is based directly on experimental data. Depths were estimated as described in the section "Results."

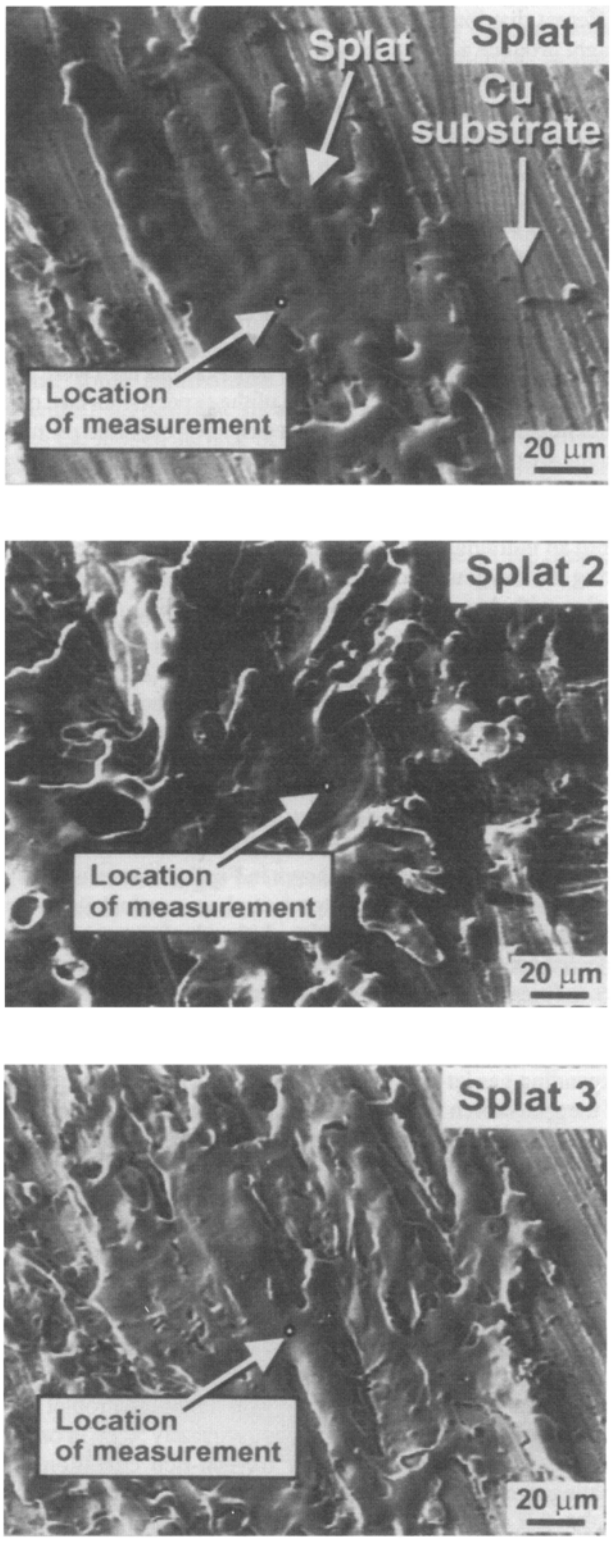

Fig. 4 SEM micrographs showing the splats corresponding to the data in Fig. 3 and the measurement locations. The diameter of the measurement region was ~ 1 μm.

concentration at the splat-substrate boundary was also observed, presumably due to residual oxide on the substrate surface. This small oxygen peak provided further confirmation that the substrate had been reached via the sputtering process.

3. Results

Concentration profiles for three individual splats on copper substrates are shown in Fig. 3. All three splats show an oxide layer on the top surface (the side away from the substrate) with a semi quantitative composition of approximately of 50 at.% iron and 50 at.% oxygen (i.e., apparently FeO). This is consistent with x-ray diffraction (XRD) analyses that show that the oxide in these sprayed coatings is primarily FeO.

The estimated depths in Fig. 3 were computed on the basis of the measured sputter rate of 21.7 nm/min for our silica reference standard. It is believed that the true sputtering rates of Fe and FeO may be somewhat greater than that of silica (Ref 12), and the actual thicknesses of the oxide and iron layers may, therefore, be somewhat greater than the estimates indicated in Fig. 3. Unfortunately, no data were available to provide a reliable estimate of the true sputter rates for the Fe and FeO phases under the conditions of this study. Nevertheless, as discussed later in this paper, the thickness estimates resulting from the assumed 21.7 nm/min sputter rate seem to be quite reasonable when compared to actual oxide and splat thicknesses observed in polished cross sections of coatings sprayed under these conditions.

If we define 75 at.% Fe/25 at.% O (i.e., the halfway point in the transition from FeO to Fe) as the iron oxide/iron interface, then the oxide layers on Splats 1 & 3 are approximately 0.7 and 1.6 microns thick respectively. The oxide layer on Splat 2 has a pronounced iron-rich region in the middle of the layer, and the total thickness of the Splat 2 oxide layer is ~1 μm.

The width of the transition region from iron to copper varies greatly among the three splats. This transition occurs over an estimated range of 2 μm for Splat 1, 6 μm for Splat 2, and 9 μm for Splat 3. A slight peak in the oxygen concentration associated with the initial rise in Cu concentration probably indicates the presence of residual copper oxide from the original surface of the substrate. Using this small oxygen peak as an indicator of the original splat/substrate interface, the total thicknesses of Splats 1, 2, and 3 are approximately 6, 10, and 3 μm respectively.

Scanning electron microscope (SEM) pictures of the three splats with markers indicating the locations of the Auger analyses are shown in Fig. 4. These splats were deliberately chosen to sample a range of apparent splat morphologies. Splat 1 shows the least evidence of splashing, with no apparent surface debris and relatively uniform flow. Splat 2 appears to have experienced much greater splashing and the original photomicrograph showed evidence of some finer particles on the surface of the splat (apparently due to redeposition of splashed material). Splat 3 appears to be somewhat intermediate in its structure and flow characteristics. In each case, the region for analysis was selected on the basis that the local surface was relatively uniform and flat with no apparent structure or foreign material within several beam diameters of the measurement location.

Figure 5 shows iron and oxygen depth profiles for a splat deposited on an aluminum substrate. This was the first sample measured and the substrate element composition was not monitored as a means to positively detect breakthrough into the substrate. However, both the iron and oxygen signals began to fall off rapidly at approximately 225 min, indicating crossing over into the substrate material. The important feature of Splat 4 is that it lacks the micron-thick oxide layer on the top surface, yet there is clearly an oxygen rich layer (~75 at.% Fe/25 at.% O) at the base of the splat adjacent to the substrate. This composition lies in the midst of a two-phase region between pure Fe and FeO (wustite) above 560 °C, and between pure Fe and Fe_3O_4 (magnetite) below 560 °C (Ref 9). It is possible that the oxide-rich region on the bottom side of Splat 4 may actually be a two-phase mixture, where the individual phases may be submicron in size, that is, too small to be individually resolved by the ~1 μm AES spot size.

4. Discussion

The purpose of the Auger spectroscopy measurements was to examine the top surface of individual droplets for the presence of an oxide layer that may have formed after the droplet flattened and to determine the distribution of oxygen through the thickness of the splat. The disadvantage of this approach is that only a small number of splats could be examined because of the long times required to ion mill through the specimens. To complement the Auger data, metallographic cross sections of coatings sprayed onto aluminum substrates at the same torch conditions were prepared. The advantage of the cross sections is that a large number of splats can be more easily examined to help evaluate possible oxide formation mechanisms. However, except for the first and last layers of a sprayed deposit, the relative position of the oxide layers observed in between metal layers in metallographic sections could not be clearly determined; i.e., it can be questioned whether a given oxide layer actually forms on the top of the underlying splat or the bottom of the overlying splat.

X-ray diffraction data show that the sprayed coatings contain ferrite (α-Fe) and wustite (FeO). A careful examination of the lattice parameters shows that very little oxygen (<0.1 wt%) is dissolved in the iron. The wustite is a defect oxide of the form $Fe_{1-x}O$. Lattice parameter data suggests that $0.06 < x < 0.08$. The phase diagram shows that liquid Fe and FeO are immiscible. At 2000 K the Fe will dissolve ~0.35 wt% oxygen. Therefore, during cooling it is possible that a small amount of FeO (~0.5%) can precipitate within the Fe. The FeO is unstable below 833 K and eventually will decompose to form magnetite (Fe_3O_4) and ferrite. However, during rapid cooling the FeO does not transform and remains at room temperature as a metastable phase.

The oxidation of solid iron at high temperatures begins with the formation of an FeO layer with Fe_3O_4 and Fe_2O_3 forming sequentially in layers around the FeO (Ref 11). At 1300 K the FeO typically constitutes ~95% of the total oxide layer. The FeO percentage increases at higher temperatures. The diffusion of Fe through the oxide layer is the rate limiting step for solid state oxidation. Since FeO results from both solid state and liquid state oxidation reactions, it is difficult to use phase and composition information alone to study the oxidation process. An examination of the coating microstructure in combination with analytical estimates of oxide thicknesses can help evaluate the relative importance of oxidation after the droplet has flattened.

4.1 Oxidation Model

Since diffusion of Fe through FeO is the rate limiting step in solid state oxidation (Ref 13,14), a parabolic growth law with a temperature-dependent rate constant, k, can be used to describe the oxidation progression. This can be expressed as:

$$\delta^2 = 2kt \qquad \text{Eq 1}$$

where δ is the oxide thickness and t is time.

The parabolic rate can be estimated by calculating the iron diffusion rate through the oxide. Kofstad (Ref 14) provides a functional form for this diffusion coefficient. This was obtained from Himmel et al. (Ref 15). Unfortunately, Himmel et al. contained a typographical error in this relation, which was copied into Kofstad. The correct equation for the diffusion coefficient (D) is:

$$D = 1.18 \times 10^{-6} \exp\left(\frac{-29{,}700 \dfrac{\text{cal}}{\text{mol}}}{RT}\right) \frac{\text{m}^2}{\text{s}} \qquad \text{Eq 2}$$

which is in an Arrhenius form where R is the gas constant and T is temperature. This value of the diffusion coefficient can be used in place of k in Eq 1, and yields an oxide thickness of 0.15 μm for iron at 1300 K for 1 ms. This is of the same order of magnitude as that obtained from a plot given by Birks and Meier (Ref 13). This plot indicates that at 1300 K iron will develop a 0.04 μm layer of oxide in 1 ms. Samonov (Ref 16) also gives a value of k to be used in Eq 1.

$$D = 2.4 \times 10^{-6} \exp\left(\frac{-40{,}000 \dfrac{\text{cal}}{\text{mol}}}{RT}\right) \frac{\text{m}^2}{\text{s}} \qquad \text{Eq 3}$$

Using Eq 3 yields an oxide thickness of 0.03 μm for the 1 ms example above. Equation 3 may provide a better estimate of the oxide growth, because the experimental basis for Eq 3 was actual oxide growth while Eq 2 was based on diffusion measurements. However, the general agreement between Eq 2 and 3 allows extending the empirically determined rate law to oxidation times outside of the range of experimental data.

The above calculations apply to an isothermal oxidation event. A proposed quasi-steady state model to simulate the oxidation during a thermal transient involves the differential equation describing the diffusion process:

$$\frac{d\delta}{dt} = \frac{k\Delta C}{\delta} \qquad \text{Eq 4}$$

where ΔC is the iron concentration difference across the oxide layer (unity).

Equation 3 gives k as a function of temperature. In order to numerically integrate Eq 4, it is necessary to define a thermal transient for splat cooling, so that k can be expressed as a function of time. We will assume that the splat cools from 1800 K to 500 K in a linear manner over 10 μs. This is consistent with splat cooling rates measured for plasma sprayed processes (Fantassi et al., Ref 17 and Moreau et al. Ref 18). However, we are implicitly assuming that the droplet is not superheated at impact and that it instantly solidifies (i.e., the time required for solidification is negligibly short in comparison to the total time for oxidation). Numerical integration of Eq 4, using Eq 3 for the parabolic constant, yields an oxide layer of 0.010 μm.

4.2 Auger Spectroscopy

If oxidation occurs after the droplet has flattened, it is reasonable to expect that the top surface of each splat should have an oxide layer whose thickness should be measured in thousandths of a micron, or perhaps more if some of the oxidation takes place on the surface of the flattened molten pool before the splat solidifies.

Splats 1, 2, and 3 clearly exhibit a thick oxide layer on their surfaces. The conservatively estimated oxide layer thickness of 1 micron is 100× greater than the calculated value. Splat 4 does not have a thick oxide layer on its top surface. However, Fig. 5 shows that a very thin oxide layer was observed. This layer was removed during the first ion milling step and is clearly very thin. Its composition is close to FeO, the oxide phase that is expected to form at high temperatures.

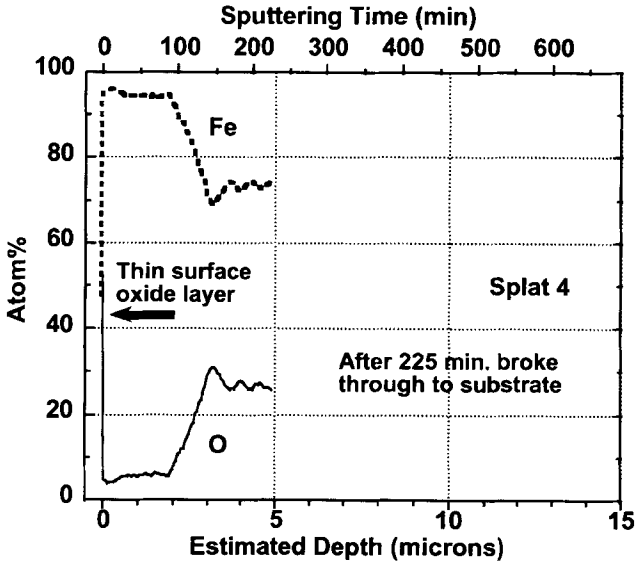

Fig. 5 Concentration profiles through a splat on an aluminum substrate. Aluminum concentration was not monitored.

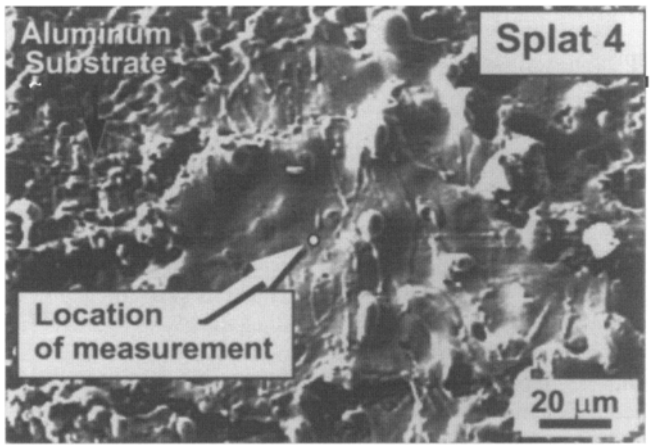

Fig. 6 SEM micrographs showing the splat corresponding to the data in Fig. 5 and the Auger measurement location

Other than the fact that the substrate was aluminum instead of copper, the spray conditions for Splat 4 were the same as those used for Splats 1 to 3. Splat 4 morphology shows that it arrived at the substrate in a fully molten state and flowed out well upon impact (Fig. 6). The thin oxide film on the top of Splat 4 is consistent with model predictions for oxidation of a droplet after impact and solidification.

4.3 Splat Microstructure within Coatings

To further examine the splat oxidation process, coatings were sprayed onto aluminum substrates and examined metallographically. High magnification micrographs showing typical alternating metal/oxide layers are shown in Fig. 7 and 8. The bright phase in these micrographs is Fe, the dark gray regions are FeO, and the black regions are voids in the sample. For the well-defined splats, the micrographs show that the thickness of the metal layers varies from several microns up to nearly 10 μm thick. The oxide layers, between the metal layers, are somewhat thinner. The observed range of thicknesses is consistent with the thicknesses obtained in the AES experiments. Some regions of the microstructure contain very convoluted mixtures of micron- and submicron-size Fe and FeO (lower left quadrant of Fig. 8, for example). If such a two-phase region were encountered during ion milling, then a non-stoichiometric iron/oxygen ratio, such as that seen in the oxide-rich region of Splat 4 (Fig. 5), could result.

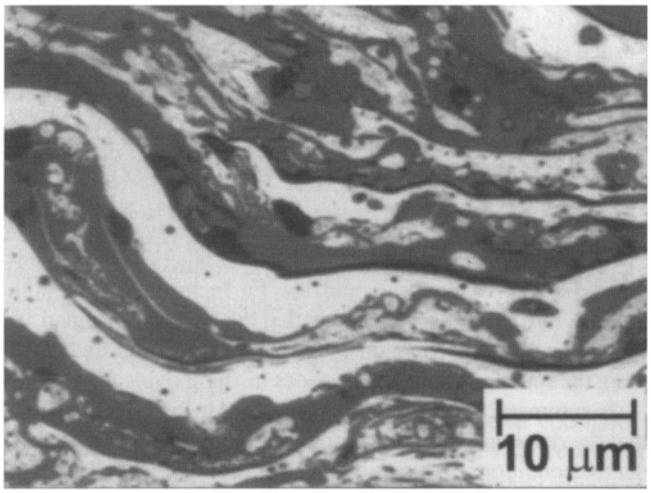

Fig. 7 Typical alternating layers of Fe (light) and FeO (dark gray) with some voids (black)

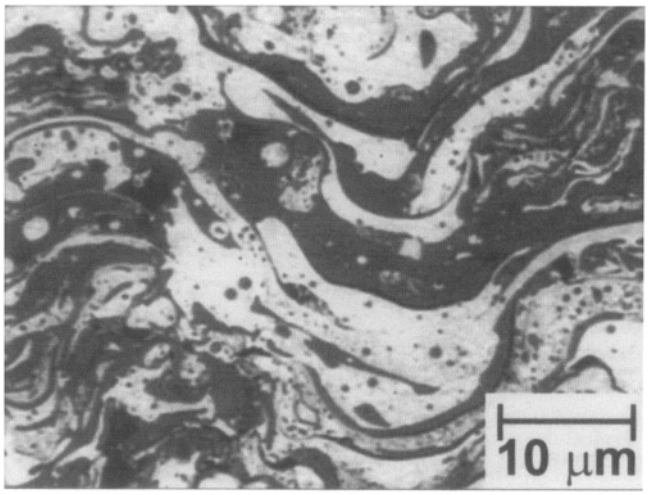

Fig. 8 Lower left corner of this micrograph shows a highly convoluted region of very fine Fe and FeO.

A very interesting and important feature apparent in the splat microstructure is the presence of very fine, approximately spherical, inclusions of Fe in the FeO and of FeO in the Fe. These spherical inclusions are very common in the splats. Examples of both types of inclusions are shown in Fig. 9. More examples abound in the other micrographs as well. The sharp iron-rich peak near the center of the oxide layer on Splat 2 is likely to have been caused by one of these Fe inclusions (Fig. 3).

Because of the spherical shape of the Fe and FeO inclusions and the immiscibility of these two phases, it seems reasonable to conclude that the Fe inclusions in the FeO (and the FeO inclusions in the Fe) formed while both phases were molten. That is, the oxide layer does not appear to have formed by a solid state diffusion process after the droplet flattens out and solidifies. It may be possible that the oxide layer forms in a molten pool on the surface of the steel splat prior to solidification; however, the solidification time is short (Ref 19), and it is difficult to provide a mechanism for forming suspended, spheroidal pockets of Fe in the FeO. A more logical explanation would seem to be that most of the FeO was already present at the time of impact as a two-phase liquid mixture of Fe and FeO. The inclusions of Fe in FeO and of FeO in Fe are likely due to the in-flight mixing action described in the Appendix, and/or they may have resulted from the

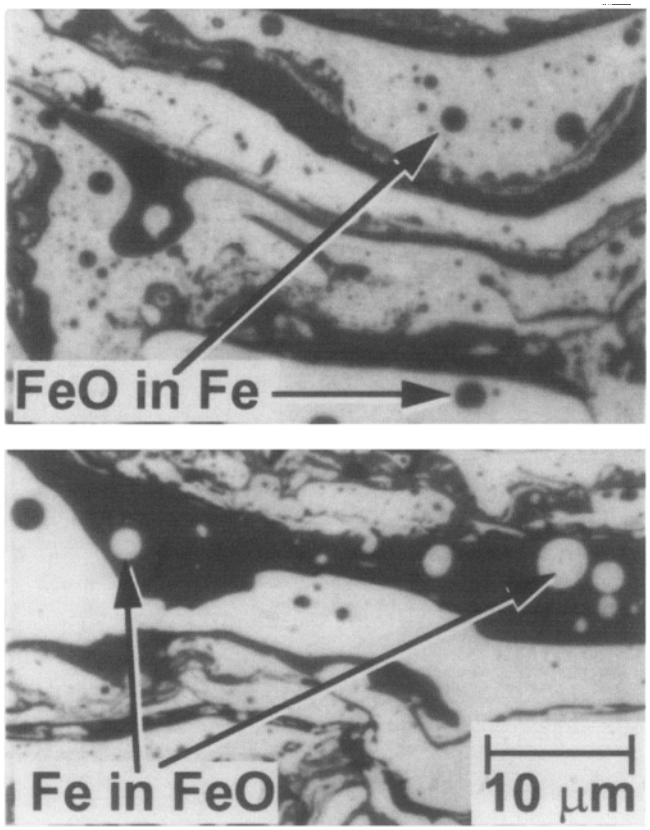

Fig. 9 Examples of ubiquitous spheroidal inclusions of FeO in Fe and Fe in FeO

violent turbulence of the impact process causing a partial mixing of the two phases.

If the pre-impact molten oxide hypothesis is correct, the coating micrographs should show examples of oxide distributions like that observed in Splat 4, i.e., metal on the top and oxide on the bottom. Figure 10a shows a region in which several splats on the top (outer surface) of the coating do not have a visible oxide overlayer. Of course, a very thin oxide overlayer, such as that found on Splat 4, would not be observed metallographically. Figure 10b shows a region in which an iron oxide layer is sandwiched between the substrate and a metal layer. Examples of metal on the top and oxide at the coating/substrate interface, such as those shown in Fig 10, were not rare occurrences. These microstructural features support the conclusion that oxidation after flattening is not the dominant mechanism in this system. Rather it supports the hypothesis that, under the conditions of this study, most of the oxidation occurs prior to impact.

5. Conclusions

A mild steel wire (AISI 1025) was HVOF-sprayed onto copper and aluminum substrates and examined using Auger spectroscopy/ion milling, x-ray diffraction, and metallography. An analytical model was also used to predict the thickness of an iron oxide layer that formed on a hot splat after impact and solidification. The purpose of the study was to determine whether most of the oxidation in this system occurs after the droplet has flattened, as has been reported for other systems.

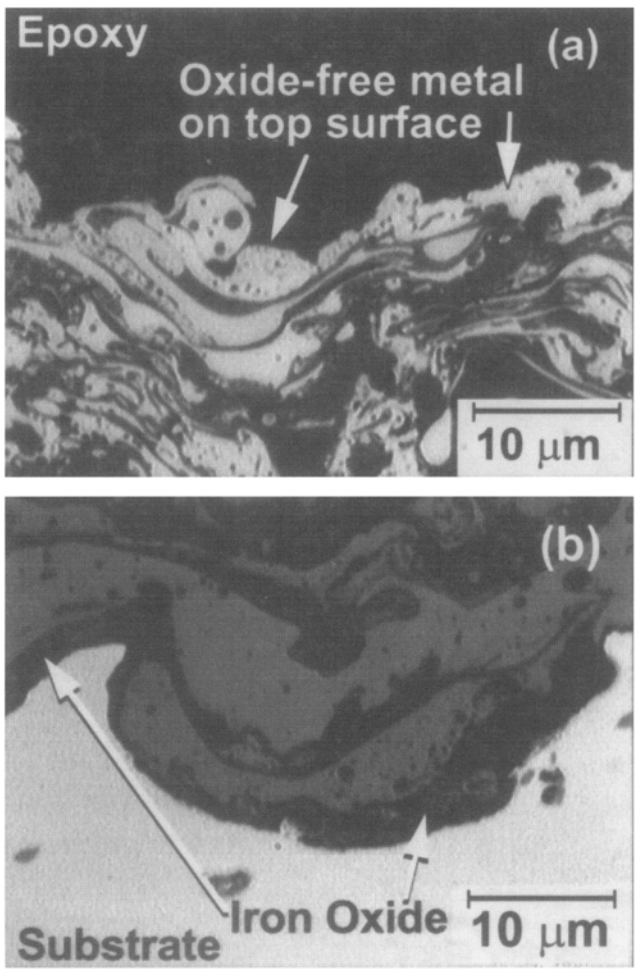

Fig. 10 Examples of (a) apparently oxide-free metal exposed on the top surface of a coating and (b) metal oxide trapped underneath a splat at the coating/substrate interface

The sprayed material consisted of a two phase mixture of ferrite (α-Fe) and wustite (FeO). These two materials are immiscible in one another as liquids. AES measurements were made on several individual splats. In three of the splats, a thick oxide layer on top of a metal layer was observed. The oxide layer had a composition close to that of FeO. The estimated thickness of the oxide was ~1 μm. The calculated oxide thickness, assuming that all the oxidation occurred after solidification, is only 0.010 μm (i.e., two orders of magnitude thinner than the oxides observed in Splats 1 to 3). In a fourth splat, the metal layer was on top of an iron oxide layer with the oxide immediately adjacent to the substrate.

Metallographic examination of coating cross sections revealed alternating layers of Fe and FeO (see Fig. 7, 8). The thicknesses of the oxide and metal layers are similar to those obtained using Auger spectroscopy. Numerous regions in the coating microstructure could be found where the last layer of splats deposited (i.e., the top surface of the coating) did not have an oxidized overlayer (Fig. 10a). The presence of these unoxidized splats shows that Splat 4 was not atypical. Regions at the bottom of the coating, where the first layer of splats was put down, showed examples of an iron oxide layer immediately adjacent to the substrate (Fig. 10b).

The presence of micron and submicron, nearly spherical, inclusions of Fe suspended within the FeO layers strongly suggests that the oxide layer and the Fe inclusions were both molten. That is, it does not appear that the FeO layer formed after impact. No reasonable mechanisms could be proposed to explain the spherical inclusions besides in-flight oxide formation.

In summary, the observations presented in this paper indicate that the dominant mechanism for forming intersplat oxides under the conditions of this study is in-flight oxidation and not oxidation of the splats after they flatten. A primary difference between this study and previous investigations is the use of a wire fed spray device as opposed to powder fed spray devices.

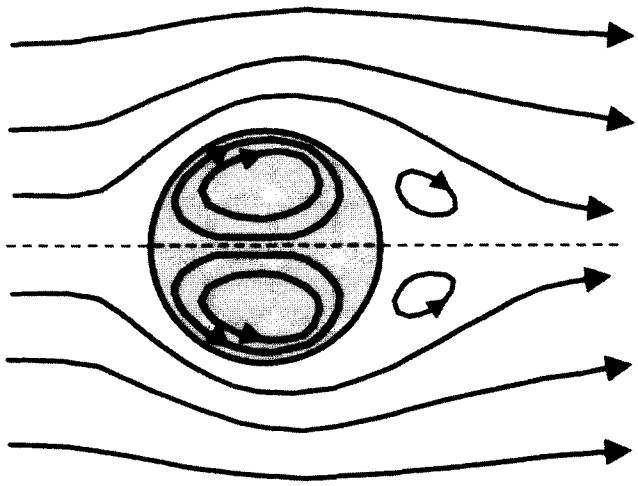

Fig. 11 Toroidal flow within a fully molten droplet is stimulated by shear forces due to high-velocity gas flow around the droplet.

6. Appendix

It is of interest to estimate how much fluid motion is induced in a molten metal drop exposed to a fast moving gas stream. This would help in determining if an oxide layer could form on the outside of a molten drop that would inhibit further oxidation. In an article in the Journal of the Atmospheric Sciences, LeClair et al. (Ref 20) calculate the induced velocities in a water drop traveling through air. Using a numerical method to calculate velocities in both the air and the water, LeClair et al. show that the maximum velocity occurs slightly upstream of the drop equator. This maximum velocity is determined to be a function of the Reynolds number (based on the droplet diameter, the relative velocity, and the gas kinematic viscosity), the density ratio, and the viscosity ratio.

Based on these observations, a toroidal flow field may be established within a molten droplet as the higher velocity gas flows past the slower moving droplet. The resulting flow pattern within the droplet is shown schematically in Fig. 11.

In the HVOF application described in this paper, the Reynolds number is around 200 for combustion gas flow past the 50 μm iron droplets. LeClair et al. report that the maximum liquid velocity would be about 4% of the relative gas velocity for their water/air system at this Reynolds number. Also, LeClair et al. show that the results are, to first order, proportional to the dynamic viscosity ratio of the two fluids. For water and air, the viscosity ratio is approximately 55. For our system, the viscosity ratio is approximately 130. Thus, the maximum velocity for our system is 2% of the relative gas velocity.

If the relative gas velocity is 1000 m/s, then the maximum liquid surface velocity is estimated at 20 m/s, and the average liquid velocity is estimated at 10 m/s. Thus, the liquid moves a distance equal to the diameter of the particle (50 μm) in 5 μs. During this time, the liquid particle has moved approximately 0.5 mm down the plume.

This example indicates that the liquid motion constantly sweeps fresh fluid to the surface of the particle. This fresh fluid is then available for oxidation. Thus a diffusion model similar to that presented in this paper will not predict in-flight oxidation.

Acknowledgments

The authors wish to acknowledge valuable contributions by T.J. Roemer and J.W. Cates with sample preparation, T.W. Grasser and J.E. Brockmann with the PDPA measurements, D.T. McGuffin with metallography, and R.W. Buttry with the Auger spectroscopy/ion milling analyses. Sandia National Laboratories is operated by Lockheed Martin for the U.S. Department of Energy under contract DE-AC04-94AL85000.

References

1. S.E. Hartfield-Wunsch and S.C. Tung, The Effect of Microstructure on the Wear Behavior of Thermal Spray Coatings, *Thermal Spray Industrial Applications,* C.C. Berndt and S. Sampath, Ed., ASM International, 1994, p 19-24
2. W.D. Swank, J.R. Fincke, D.C. Haggard, G. Irons, and R. Bullock, HVOF Particle Flow Field Characteristics, *Thermal Spray Industrial Applications,* C.C. Berndt and S. Sampath, Ed., ASM International, 1994, p 319-324
3. G.K. Creffield, M.A. Cole, and G.R. White, The Effect of Gas Parameters on HVOF Coatings, *Thermal Spray Science & Technology,* C.C. Berndt and S. Sampath, Ed., ASM International, 1995, p 291-296
4. C.M. Hackett and G.S. Settles, Research on HVOF Gas Shrouding for Coating Oxidation Control, *Thermal Spray Science & Technology,* C.C. Berndt and S. Sampath, Ed., ASM International, 1995, p 21-29
5. C.M. Hackett and G.S. Settles, Turbulent Mixing of the HVOF Thermal Spray and Coating Oxidation, *Thermal Spray Industrial Applications,* C.C. Berndt and S. Sampath, Ed., ASM International, 1994, p 19-24
6. K. Korpiola, J.-P. Hirvonen, H. Jalkanen, L. Lass, and F. Rossi, Oxygen Partial Pressure Measurement in the HVOF Gun Tail Flame, *Thermal Spray Science & Technology,* C.C. Berndt and S. Sampath, Ed., ASM International, 1995, P 181-185
7. A. Vardelle, P. Fauchais, and N.J. Themelis, Oxidation of Metal Droplets in Plasma Sprays, *Thermal Spray Science & Technology,* C.C. Berndt and S. Sampath, Ed., ASM International, 1995, p 175-180
8. R.A. Neiser, J.E. Brockmann, T.J. O'Hern, R.C. Dykhuizen, M.F. Smith, T.J. Roemer, and R.E. Teets, Wire Melting and Droplet Atomization in a HVOF Jet, *Thermal Spray Science & Technology,* C.C. Berndt and S. Sampath, Ed., ASM International, 1995, p 99-104
9. G.J. Shubat, M.B. Bever, and T. Lyman, Ed., *Metals Handbook,* 8th ed., Vol 8, ASM International, 1973, p 304
10. A.R. Lopez, B. Hassan, W.L. Oberkampf, R.A. Neiser, T.J. Roemer, Computational Fluid Dynamics of a Wire-Feed, High-Velocity Oxygen-Fuel (HVOF) Thermal Spray Torch, *Thermal Spray: Practical Solutions for Engineering Problems,* C.C. Berndt, Ed., ASM International, 1996, p 531-540
11. R.A. Neiser, J.E. Brockmann, T.J. O'Hern, R.C. Dykhuizen, M.F. Smith, T.J. Roemer, and R.E. Teets, Wire Melting and Droplet Atomization in an HVOF Jet, *Thermal Spray Science & Technology,* C.C. Berndt and S. Sampath, Ed., ASM International, 1995, p 99-104
12. D. Briggs and M.P. Seah, Ed., *Practical Surface Analysis by Auger and X-Ray Photoelectron Spectroscopy,* John Wiley & Sons, 1983, p 213
13. N. Birks and G.H. Meier, *Introduction to High Temperature Oxidation of Metals,* Edward Arnold Ltd., London, 1983
14. P. Kofstad, *High Temperature Oxidation of Metals,* John Wiley & Sons, 1966
15. L. Himmel, R.F. Mehl, and C.E. Birchenall, Self Diffusion of Iron in Iron Oxides and the Wagner Theory of Oxidation, *Trans. AIME,* 197, 1953, p 827
16. G.V. Samsonov, *The Oxide Handbook,* IFI/Plenum, 1973
17. S. Fantasi, M. Vardelle, A. Vardelle, and P. Fauchais, Influence of the Velocity of Plasma Sprayed Particles on the Splat Formation, *Thermal Spray Research, Design and Applications,* C.C. Berndt and T.F. Bernecki, Ed., ASM International, 1993, p 1-6
18. C. Moreau, P. Cielo, M. Lamontagne, Flattening and Solidification of Thermal Sprayed Particles, *Thermal Spray: International Advances in Coatings Technology,* C.C. Berndt, Ed., ASM International, 1992, p 761-766
19. C. Moreau, M. Lamontagne, P. Cielo, Influence of the Coating Thickness on the Cooling Rate of Plasma-Sprayed Particles Impinging on a Substrate, *Thermal Spray Coatings: Properties, Processes and Applications,* T.F. Bernecki, Ed., ASM International, 1991, p 237-243
20. B.P. LeClair, A.F. Hamilee, H.R. Pruppacher, and W.D. Hall, A Theoretical and Experimental Study of the Internal Circulation in Water Drops Falling at Terminal Velocity in Air, *J. Atmospheric Sciences,* 29, 1972, p 728-740